

# Polyhedral Oligomeric Silsesquioxane Nanocomposite Thin Films via Layer-by-layer Electrostatic Self-Assembly

Guojun Wu and Zhaohui Su\*

State Key Laboratory of Polymer Physics and Chemistry, Changchun Institute of Applied Chemistry, Chinese Academy of Sciences, and Graduate School of the Chinese Academy of Sciences, 5625 Renmin Street, Changchun 130022, People's Republic of China

Received March 31, 2006. Revised Manuscript Received May 18, 2006

Fabrication of ultrathin polymer composite films with low dielectric constants has been demonstrated. Octa(aminophenyl)silsesquioxane (OAPS) was synthesized and assembled with poly(acrylic acid) (PAA) and poly(styrene sulfonate) (PSS) via a layer-by-layer electrostatic self-assembly technique to yield nanoporous ultrathin films. The OAPS was soluble in water at pH 3 or lower, and suitable pH conditions for the OAPS/PAA and OAPS/PSS assemblies were determined. The multilayer formation process was studied by contact angle analysis, X-ray photoelectron spectroscopy, atomic force microscopy, quartz crystal microgravimetry, UV–vis spectroscopy, and ellipsometry. The multilayer growth was found to be steady and uniform, and the analysis of the film surface revealed a rough topography due to OAPS aggregates. The incorporation of porous OAPS molecules into the thin films significantly lowered their dielectric constants. The OAPS/PAA multilayer thin film thus prepared exhibited a dielectric constant of 2.06 compared to 2.58 for pure PAA film. The OAPS/PAA multilayer film was heated to effect cross-linking between the OAPS and the PAA layers, and the transformation was verified by reflection–absorption Fourier transform infrared spectroscopy. The stability of the film was found to significantly improve by the cross-linking via amide formation.

## Introduction

The continuous advancement of microelectronics has led to integrated circuits of decreasing feature sizes, which demand new interlayer dielectric materials with lower dielectric constants (low- $\kappa$ ) to reduce signal delay and improve performance.<sup>1,2</sup> Therefore, the search for low- $\kappa$  materials, in particular polymers suitable for interlayer application, has attracted a great deal of attention. A polymer's dielectric constant can be effectively reduced by incorporation of pores into the polymer film, because the dielectric constant of air is  $\sim 1$ .<sup>1</sup> For example, nanoporous polyimide films have been prepared from copolymers of polyimides and poly(propylene oxide) (PPO), where they phase separate and the spherical PPO domains are thermally degraded, leaving pores of tens of nanometer size,<sup>3–5</sup> and with certain fluorinated polyimide a dielectric constant as low as 2.3 has been reported.<sup>5</sup> However, the pores thus formed may collapse as a result of the high surface tension of the pores.<sup>1,4</sup> Another approach is to incorporate into the polymer chains moieties with nanopores, such as the octamer [RSiO<sub>1.5</sub>]<sub>8</sub> of the polyhedral oligomeric silsesquioxane (POSS) family, which is a rigid cubic cage with a pore of

$\sim 0.3$  nm size.<sup>6</sup> It has been demonstrated that incorporation of POSS into some polymers can enhance their mechanical properties and thermal stability.<sup>7,8</sup> Furthermore, recent studies have shown that polyimides with POSS moieties as chain ends,<sup>9</sup> pendant groups for the main chains,<sup>10</sup> and grafted side chains<sup>11</sup> exhibit lower dielectric constants than the corresponding polyimide homopolymers, and the dielectric constant of the composite can be tuned by adjusting the amount of POSS incorporated.

In the fabrication of integrated circuits, polymer dielectrics can be deposited by techniques such as spin coating and chemical vapor deposition to yield thin layers.<sup>1,2</sup> On the other hand, one promising method for fabricating supported organic thin films is the layer-by-layer self-assembly technique,<sup>12–14</sup> which is based on the balance between the adsorption and desorption of charged molecules at the solution/substrate interface.<sup>15</sup> The technique has proved to be a rapid and versatile method for preparing multilayer thin

\* Corresponding author. Tel.: +86-431-5262854. Fax: +86-431-5262126. E-mail address: zhsu@ciac.jl.cn.

(1) Maier, G. *Prog. Polym. Sci.* **2001**, *26*, 3.

(2) Treichel, H.; Ruhl, G.; Ansmann, P.; Würfl, R.; Müller, C.; Dietlmeier, M. *Microelectron. Eng.* **1998**, *40*, 1.

(3) Charlier, Y.; Hedrick, J. L.; Russell, T. P.; Jonas, A.; Volksen, W. *Polymer* **1995**, *36*, 987.

(4) Hedrick, J. L.; Russell, T. P.; Labadie, J.; Lucas, M.; Swanson, S. *Polymer* **1995**, *36*, 2685.

(5) Carter, K. R.; DiPietro, R. A.; Sanchez, M. I.; Swanson, S. A. *Chem. Mater.* **2001**, *13*, 213.

(6) Zhang, C. X.; Babonneau, F.; Bonhomme, C.; Laine, R. M.; Soles, C. L.; Hristov, H. A.; Yee, A. F. *J. Am. Chem. Soc.* **1998**, *120*, 8380.

(7) Huang, J. C.; He, C. B.; Xiao, Y.; Mya, K. Y.; Dai, J.; Siow, Y. P. *Polymer* **2003**, *44*, 4491.

(8) Choi, J.; Tamaki, R.; Kim, S. G.; Laine, R. M. *Chem. Mater.* **2003**, *15*, 3365.

(9) Leu, C. M.; Reddy, G. M.; Wei, K. H.; Shu, C. F. *Chem. Mater.* **2003**, *15*, 2261.

(10) Leu, C. M.; Chang, Y. T.; Wei, K. H. *Macromolecules* **2003**, *36*, 9122.

(11) Chen, Y. W.; Kang, E. T. *Mater. Lett.* **2004**, *58*, 3716.

(12) Decher, G. *Science* **1997**, *277*, 1232.

(13) Zhang, X.; Gao, M. L.; Kong, X. X.; Sun, Y. P.; Shen, J. C. *Chem. Commun.* **1994**, 1055.

(14) Kong, W.; Zhang, X.; Gao, M. L.; Zhou, H.; Li, W.; Shen, J. C. *Macromol. Rapid Commun.* **1994**, *15*, 405.

(15) Linford, M. R.; Auch, M.; Möhwald, H. *J. Am. Chem. Soc.* **1998**, *120*, 178.

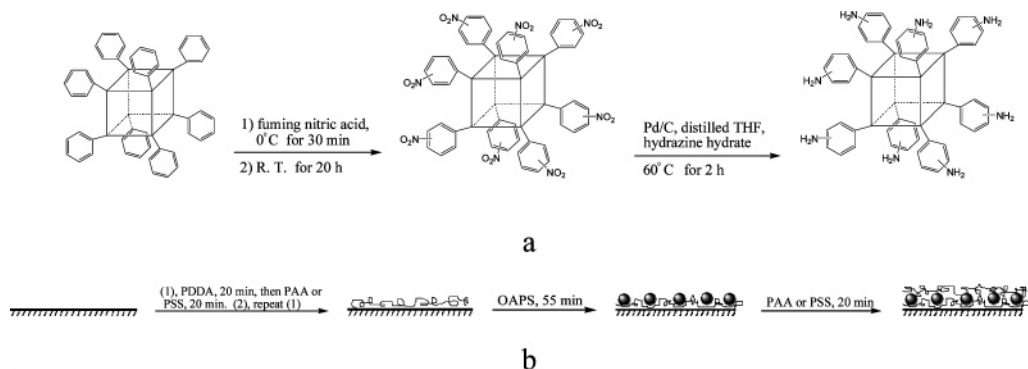


**Figure 1.** Schematic illustrations of the synthesis of OAPS (a) and stepwise growth of OAPS/PAA or OAPS/PSS multilayer films (b).

films, including some functional materials.<sup>16–18</sup> The structure, thickness, and composition of the thin film can be affected by ionic strength, polymer concentration, solution pH, deposition time, and so forth,<sup>19,20</sup> and a variety of species have been successfully assembled using this technique, such as dyes,<sup>21,22</sup> proteins,<sup>23</sup> DNA,<sup>24</sup> viruses,<sup>25</sup> and inorganic materials.<sup>26</sup> Different kinds of substrates of various shapes can be used, and after the layer-by-layer assembly process is done, the film may be treated further to affect structural transformation.<sup>27</sup> An interesting example is the assembly of poly(styrene sulfonate) (PSS) and octa(3-aminopropyl)silsesquioxane onto planar substrates and polystyrene particles, where composite multilayers were produced.<sup>28</sup> However, the POSS used in that study was a mixture including incompletely condensed octamers and other species, which is not desirable for producing nanoporous composite films, and the thin films can easily delaminate from the substrates.<sup>28</sup>

In the present study, we choose octa(aminophenyl)silsesquioxane (OAPS) as our POSS building block to produce nanocomposite films with poly(acrylic acid) (PAA) or PSS via layer-by-layer assembly. The approach is illustrated in Figure 1. First OAPS is synthesized following a procedure reported in the literature<sup>29</sup> with some modification. The amine groups on the OAPS make it readily soluble in water under acidic conditions as a polycation, and the layer-by-layer self-assembly with PAA or PSS can be easily realized in aqueous media. In the case of the OAPS/PAA nanocomposite, the film is further heated to effect cross-

linking between OAPS and PAA to improve its stability. The assembly process was studied with quartz crystal microgravimetry, UV–vis spectroscopy, contact angle analysis, X-ray photoelectron spectroscopy (XPS), and ellipsometry, and the heat treatment of the OAPS/PAA films was investigated by reflection–absorption Fourier transform infrared (FTIR) spectroscopy.

## Experimental Section

**Materials.** PAA ( $M_w = 2000$ ), octaphenylsilsesquioxane (OPS), PSS ( $M_w = 70000$ ), and poly(diallyldimethylammonium chloride) (PDDA), 20 wt % in water ( $M_w = 200\,000$ – $350\,000$ ), were purchased from Aldrich and used as received. Polished silicon wafers were purchased from Wafer Works Corporation (Shanghai, China). Deionized water ( $18.2\text{ M}\Omega\cdot\text{cm}$ ) used for rinsing and preparing all the solutions was obtained from a Millipore Simplicity 185 purification unit.

**Synthesis of Octa(nitrophenyl)silsesquioxane (ONPS).** ONPS was synthesized by following the procedure reported by Laine et al.<sup>29</sup> To 25 mL of fuming nitric acid was added 5.01 g of OPS (4.85 mmol) in small portions at 0 °C with stirring. The solution was stirred for 30 min at 0 °C and then at room temperature for 20 h after the addition of OPS was complete. The mixture was filtered, the solution was poured onto 30 g of ice, and a precipitate of lightly yellow color was obtained. The precipitate was washed with water to pH  $\approx 7$  and then with ethanol three times. The powder obtained was dried under vacuum at room temperature. Yield 6.1 g (4.37 mmol, 90%). <sup>1</sup>H NMR (acetone- $d_6$ , ppm): 9.1 (t, 0.2H), 8.7 (t, 1.0H), 8.4–8.0 (m, 4.1H), 8.0–7.8 (m, 2.5H). <sup>13</sup>C NMR (acetone- $d_6$ , ppm): 153.4, 148.9 (small), 148.4, 140.5, 138.1, 135.9 (small), 134.9, 133.7, 131.7 (small), 130.3, 129.0, 126.6, 124.7, 123.1 (small), 121.6 (small). Solid <sup>29</sup>Si NMR (ppm): –81.1 (PhSiO<sub>3</sub>). FTIR (cm<sup>-1</sup>): 1350 ( $\nu\text{N}=\text{O}$ ), 1530 ( $\nu\text{N}=\text{O}$ ), 1097 (Si–O–Si).

**Synthesis of OAPS.** OAPS was synthesized according Laine's method with some modification. ONPS (1.50 g, 1.07 mmol) and 10 wt % Pd/C (0.138 g, 0.13 mmol) were added to a 100 mL Schlenk flask equipped with a condenser under N<sub>2</sub>. Distilled tetrahydrofuran (THF; 30 mL) was then added, and the mixture was stirred; at room temperature, 2.4 mL of hydrazine hydrate (80%, 38 mmol) was slowly added to the flask. After the addition of the hydrazine hydrate was complete, the mixture was heated to about 60 °C. After about 1 h the mixture separated into an achromatous top layer and a black suspension in the bottom. The mixture was cooled to room temperature, to which 5 mL of distilled THF was added, and filtered through Celite. Another 5 mL of THF was added to the flask to dissolve the remaining slurry, and the suspension was filtered again. The filtrates were combined with 10 mL of ethyl acetate and washed with water (15 mL  $\times$  3). The organic layer

- (16) Chen, H.; Zeng, G. H.; Wang, Z. Q.; Zhang, X.; Peng, M. L.; Wu, L. Z.; Tung, C. H. *Chem. Mater.* **2005**, *17*, 6679.  
 (17) Zhang, X.; Shi, F.; Yu, X.; Liu, H.; Fu, Y.; Wang, Z. Q.; Jiang, L.; Li, X. Y. *J. Am. Chem. Soc.* **2004**, *126*, 3064.  
 (18) Zhang, X.; Shen, J. C. *Adv. Mater.* **1999**, *11*, 1139.  
 (19) Shiratori, S. S.; Rubner, M. F. *Macromolecules* **2000**, *33*, 4213.  
 (20) Dubas, S. T.; Schlenoff, J. B. *Macromolecules* **1999**, *32*, 8153.  
 (21) Ariga, K.; Lvov, Y.; Kunitake, T. *J. Am. Chem. Soc.* **1997**, *119*, 2224.  
 (22) Ma, N.; Zhang, H. Y.; Song, B.; Wang, Z. Q.; Zhang, X. *Chem. Mater.* **2005**, *17*, 5065.  
 (23) Liu, H. Y.; Rusling, J. F.; Hu, N. F. *Langmuir* **2004**, *20*, 10700.  
 (24) Shi, X. Y.; Sanedrin, R. J.; Zhou, F. M. *J. Phys. Chem. B* **2002**, *106*, 1173.  
 (25) Lvov, Y.; Haas, H.; Decher, G.; Mohwald, H.; Mikhailov, A.; Mchedlishvily, B.; Morgunova, E.; Vainshtein, B. *Langmuir* **1994**, *10*, 4232.  
 (26) Keller, S. W.; Kim, H. N.; Mallouk, T. E. *J. Am. Chem. Soc.* **1994**, *116*, 8817.  
 (27) Ma, N.; Wang, Y. P.; Wang, Z. Q.; Zhang, X. *Langmuir* **2006**, *22*, 3906.  
 (28) Cassagneau, T.; Caruso, F. *J. Am. Chem. Soc.* **2002**, *124*, 8172.  
 (29) Tamaki, R.; Tanaka, Y.; Asuncion, M. Z.; Choi, J.; Laine, R. M. *J. Am. Chem. Soc.* **2001**, *123*, 12416.

was dried over 5 g of  $\text{MgSO}_4$  and precipitated in 300 mL of hexane. The white precipitate was collected by filtration, redissolved in 10 mL of 30:50 THF/ethyl acetate, and precipitated in 200 mL of hexane. The powder was dried at room temperature under vacuum. Yield 0.76 g (0.66 mmol, 62%).  $^1\text{H}$  NMR (acetone- $d_6$ , ppm): 7.8–6.2 (b, 1.0H), 5.1–4.2 (b, 0.45H).  $^{13}\text{C}$  NMR (acetone- $d_6$ , ppm): 153.6, 151.6 (small), 147.9, 136.0, 132.2, 131.5 (shoulder), 128.8, 126.5 (shoulder), 119.4 (shoulder), 125.2, 122.8, 120.3, 116.9, 115.4, 113.9 (small). Solid  $^{29}\text{Si}$  NMR (ppm): –75.8 (shoulder,  $\text{PhSiO}_3$ ), –79.4 ( $\text{PhSiO}_3$ ). FTIR ( $\text{cm}^{-1}$ ): 3378 ( $\nu\text{N-H}$ ), 1122 ( $\text{Si-O-Si}$ ).

**Substrate Preparation.** Quartz slides and silicon wafers were used as substrates for film deposition and were cleaned in an 80 °C piranha solution ( $\text{H}_2\text{SO}_4\text{-H}_2\text{O}_2$  (30%) 70:30, v/v) for 40 min, rinsed with Milli-Q water, and dried with nitrogen prior to use. Glass slides were cleaned following the above steps, then coated with 15 nm of Cr and 100 nm of Au, and used as the substrates for reflection–absorption FTIR study of the assembled thin films.

**Assembly of OAPS/PAA and OAPS/PSS Composite Films.** To prepare the OAPS/PAA film, the substrate was first dipped in a PDDA aqueous solution (1 mg/mL) for 20 min, rinsed with water, and then dried with  $\text{N}_2$ . The substrate was then dipped in a PAA aqueous solution (0.01 M, repeat unit, pH = 4.5) for 20 min, then rinsed, and dried. The cycle was repeated one more time to produce a substrate with two PDDA/PAA bilayers deposited. Then the substrate was dipped in an OAPS aqueous solution (0.5 mg/mL, pH = 3.0) for 55 min, rinsed with water, and dried with  $\text{N}_2$ . The substrate was then dipped in the PAA solution for 20 min, rinsed, and dried. The deposition cycle of OAPS and PAA was repeated until a desired number of layers was obtained. For the preparation of OAPS/PSS composite films, a similar process was used, except that the PSS solution (0.01 M, repeat unit) and the water used to rinse after each PSS deposition were maintained at pH = 2.0.

**Cross-Linking of the OAPS/PAA Films.** After a composite film with nine OAPS/PAA bilayers was assembled on a PDDA/PAA-primed quartz or gold-coated glass slide, it was heated at 205 °C for 2 h under  $\text{N}_2$  to cross-link between the layers.

**Characterization.**  $^1\text{H}$  NMR and  $^{13}\text{C}$  NMR spectra were all recorded on a Bruker 300 NMR spectrometer, and the solvent was acetone- $d_6$ .  $^{29}\text{Si}$  NMR spectra were obtained on a Bruker 400 NMR spectrometer. FTIR analyses were performed using a Bruker IFS 66v/S spectrometer with the resolution maintained at 4  $\text{cm}^{-1}$ . Transmission spectra were recorded with a DTGS detector with 32 scans co-added. The reflection–absorption spectra were measured with 256 scans co-added using a mercury cadmium telluride detector and a grazing angle reflection accessory (PIKE Technologies) with the incidence angle set at 80°. Elemental analysis data were obtained from an Elementar Analysensysteme GmbH VarioEL version 4.01 analyzer.

Contact angle analyses were carried out using the static sessile drop method on a KRÜSS DSA1 version 1.80 drop shape analyzer with water as the probe liquid. Each contact angle value reported was an average of at least five measurements. UV–vis spectra of the thin films deposited on quartz slides were collected on a Shimadzu UV-2450 spectrophotometer. A homemade quartz crystal microbalance (QCM) was used to detect the mass of the deposited layer using a 9 MHz quartz electrode coated with Ag on both sides. The QCM frequency shifts were monitored with a Protek C3100 universal frequency counter, and the mass of the deposited layer was calculated from the Sauerbrey equation.<sup>30</sup> XPS spectra were obtained on a Thermo Electron ESCALAB 250 spectrometer equipped with a monochromatic Al X-ray source (1486.6 eV). The

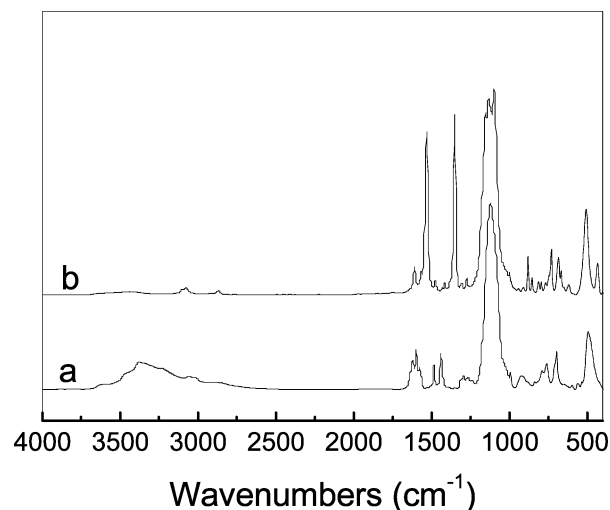


Figure 2. FTIR spectra of OAPS (a) and ONPS (b).

spectra were recorded at 90° takeoff angle with 20 eV pass energy. The sensitivity factors were obtained from standard samples for determination of atomic concentration (C 1s, 0.25; N 1s, 0.42; S 2p, 0.54; Si 2p, 0.27). Ellipsometric measurements were performed by null ellipsometry using a spectroscopic ellipsometer (HORIBA Jobin Yvon) with the scanning range of 300–800 nm and a 70° incidence angle. The refractive index of the silicon wafer was  $3.882 + 0.019i$ , and the refractive index of the silica top layer was 1.457 with the imaginary part set at zero. For each sample three points were measured, and the numbers were averaged. The atomic force microscopy (AFM) analysis was performed on a Seiko SPA300HV/SPI3800N microscope operating in tapping mode in an ambient atmosphere. A silicon cantilever (spring constant 2 N/m and resonant frequency  $\sim 70$  kHz, Olympus Co., Japan) with an etched conical tip was used for scanning.

## Results and Discussion

The OAPS was synthesized by following the method reported by Laine et al.,<sup>29</sup> which involves nitration of OPS to form ONPS followed by mild reduction (Figure 1a). The FTIR spectra of ONPS and OAPS are compared in Figure 2. It can be seen that the  $\text{N=O}$  stretching bands at 1350 and 1530  $\text{cm}^{-1}$  for ONPS completely disappear, and a broad new band due to  $\text{N-H}$  stretching appears at 3378  $\text{cm}^{-1}$ . This indicates the complete reduction of the nitro groups in the ONPS to  $\text{-NH}_2$ . This result was also confirmed by the  $^1\text{H}$  NMR data (Figure 3). For OAPS to be used as a nanopore building block, it is important that in these reactions the cubic siloxane structure remains intact. The  $^{29}\text{Si}$  NMR spectra of ONPS and OAPS are included in Figure 3, each showing a single peak at –81.1 ppm for ONPS and at –79.4 ppm for OAPS, respectively, indicating that there is only one Si species in each molecule and no destruction of the cubic siloxane cage has occurred in either the nitration or the reduction step. In the  $^1\text{H}$  NMR spectrum of the ONPS, however, a triplet is observed at 9.2 ppm, probably a result of the presence of dinitro substitution on the phenyl groups of the ONPS obtained. This is consistent with the elemental analysis result (see Supporting Information), where the N% in the ONPS is higher than the corresponding theoretical value calculated on the basis of monosubstitution of each phenyl group. On the basis of the elemental composition, it

(30) Serizawa, T.; Yamamoto, K.; Akashi, M. *Langmuir* **1999**, *15*, 4682.

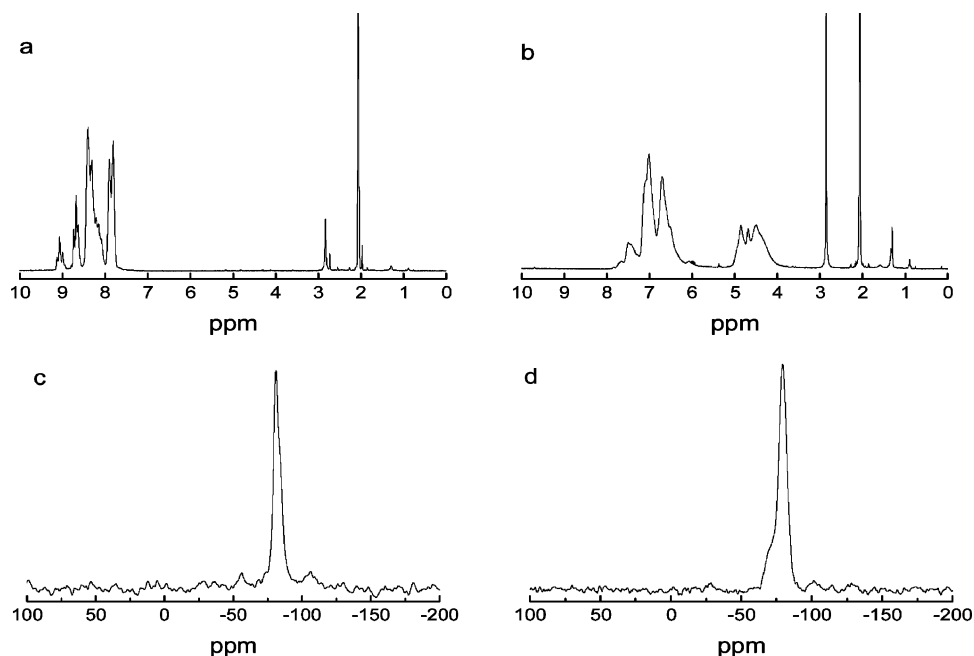


**Figure 3.**  $^1\text{H}$  NMR spectra of ONPS (a) and OAPS (b) and solid  $^{29}\text{Si}$  NMR spectra of ONPS (c) and OAPS (d).

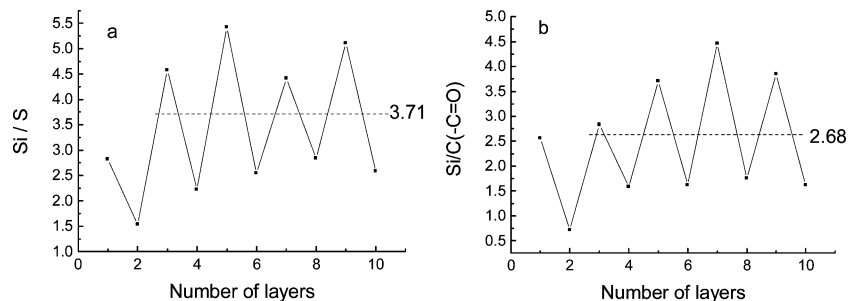


**Figure 4.** Surface atomic ratios for the multilayer films obtained by XPS: (a) Si/S for OAPS/PSS films and (b) Si/C(—C=O) for OAPS/PAA films. In each case layer 1 is OAPS.

can be estimated that there were about 5.5 mol % disubstituted phenyl groups for the ONPS, which implies the presence of the same amount of diamino phenyl groups in the OAPS. Because the extra amino groups on the OAPS can increase their charge density under acidic conditions, they are actually advantageous to the electrostatic self-assembly of the OAPS on negatively charged surfaces.

In the assembly of OAPS with PAA (Figure 1b), the solution pH proved critical. It was found that OAPS is not soluble in water until the pH is around 3, at which the aromatic amino groups are protonated. However, PAA is also a weak electrolyte, whose  $\text{p}K_a$  is 4.0–4.5 according to a previous report,<sup>31</sup> higher than the  $\text{p}K_a$  of the polycation OAPS, which should be around 3.5. This makes the pH window for OAPS and PAA solutions suitable for electrostatic self-assembly very narrow. When the OAPS solution pH was lower than 3 for OAPS deposition, it was found to cause a significant amount of desorption of PAA previously adsorbed, apparently as a result of the protonation of the carboxylate groups of the PAA and the diminishing charge association. Therefore, the OAPS solution pH in this study was maintained at 3. On the other hand, when the PAA solution pH was low at 3 or high at 5, the charge density on

the PAA to be deposited or the previously adsorbed OAPS would be low, respectively, and at pH = 4.5 the maximum amount of PAA adsorption in one layer was observed. In the case of OAPS/PSS assembly, the process is not as sensitive to the pH, because PSS is a strong electrolyte, and most of the styrene sulfonate units remain negative even at pH = 2, at which the amine groups in the OAPS are fully protonated. For this reason the pH of the PSS solution and the water used to rinse after each PSS deposition was adjusted to 2.0.

Because different substrates were used in the assembly, including quartz slides, Ag coated quartz electrodes, Si wafers, and gold coated Si wafers, two PDDA/PSS or PDDA/PAA bilayers were first assembled on the substrate to create a consistent environment for subsequent deposition of OAPS and PSS or PAA so that the characterization of the deposited films via different techniques can be compared. The layer-by-layer electrostatic assembly of OAPS and PSS or PAA was first studied by XPS and contact angle measurement. Figures 4 and 5 are the surface atomic ratios obtained by XPS and the water contact angles of the surface of the films. It can be seen clearly that the deposited layers are stratified. On the basis of the average atomic composition by XPS and the molecular weights of the repeat units, the composition of the film can be estimated. To minimize the interference

(31) Cesarano, J.; Aksay, I. A.; Bleier, A. *J. Am. Ceram. Soc.* **1988**, *71*, 250.

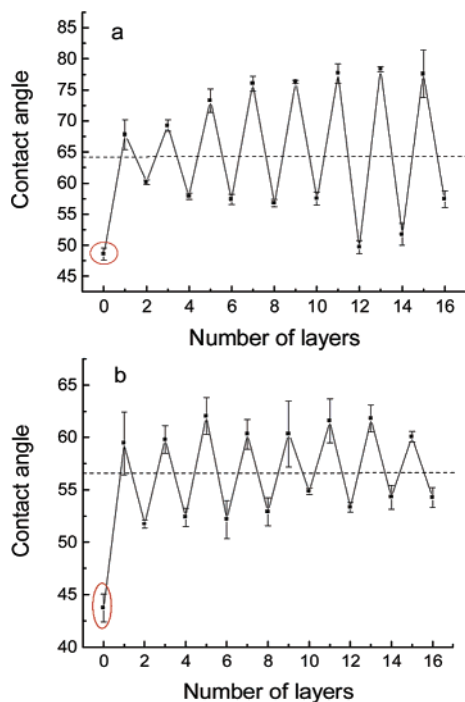


**Figure 5.** Contact angles of the OAPS/PSS (a) and OAPS/PAA (b) assembly films. The 0 layer is (PDDA/PSS)<sub>2</sub> or (PDDA/PAA)<sub>2</sub>. The odd layers are OAPS, and the even layers are PSS or PAA.

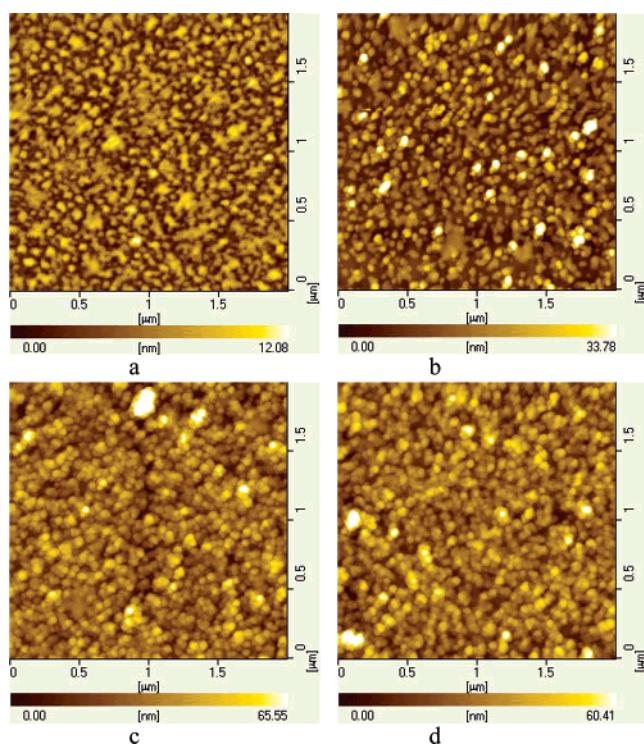


**Figure 6.** AFM images of different film surfaces: (a) (PDDA/PAA)<sub>2</sub>, RMS = 2.3 nm; (b) (PDDA/PAA)<sub>2</sub>/OAPS, RMS = 6.8 nm; (c) (PDDA/PAA)<sub>2</sub>/(OAPS/PAA)<sub>5</sub>/OAPS, RMS = 11.3 nm; and (d) (PDDA/PAA)<sub>2</sub>/(OAPS/PAA)<sub>6</sub>, RMS = 10.4 nm.

from the underlying PDDA layers, data for the top eight layers (including four OAPS and four PAA or PSS layers) were averaged. For the OAPS/PSS composite films, the average Si:S atomic ratio was 3.7:1, and the OAPS:PSS mass ratio was derived to be 72:28. For the OAPS/PAA films, the average Si:C (C=O) atomic ratio was 2.7:1, and the

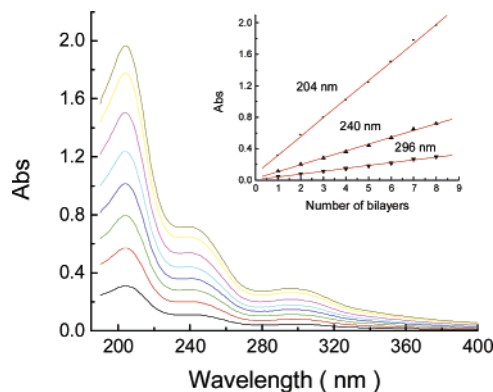


**Figure 7.** UV-vis absorption spectra of OAPS/PAA multilayer films with different numbers of bilayers deposited on quartz.

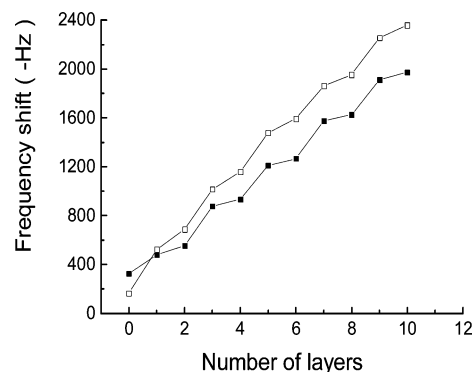


**Figure 8.** QCM frequency shifts for alternating adsorptions of OAPS and PAA (■) or OAPS and PSS (□) on a silver-coated quartz electrode. In each case the odd layers are OAPS.

OAPS:PAA mass ratio was 84:16. The surface topography of the films was assessed by AFM, and the images for films of different top layers are shown in Figure 6. With OAPS as the top layer, the surface is granular, and OAPS clusters on the order of tens of nanometers are observed (Figure 6b), which further aggregate with more layers deposited (Figure 6c). The PAA layer slightly reduces the surface roughness without changing the topography significantly, probably filling some of the gaps and the valleys between the OAPS clusters and acting like a glue to hold them together (Figure 6d). Apparently the surface morphology of the assembly films is dictated mainly by the OAPS aggregates.

The growth of the layers was monitored using UV-vis spectroscopy, and the spectra of OAPS/PAA films with different numbers of assembly cycles are shown in Figure 7. The absorbance of the E<sub>2</sub> band at 240 nm and the B band at 296 nm for the phenyl rings of the OAPS are plotted against the number of bilayers assembled, and a linear growth pattern is observed (Figure 7, inset). This indicates that the adsorption of OAPS and PAA was steady and uniform. A similar trend was found for the OAPS/PSS assembly (data not shown). The OAPS/PAA and OAPS/PSS assembly processes were investigated by quartz crystal microgravimetry, and the data are plotted in Figure 8. Regular growth of the multilayers is clearly observed for both OAPS/PAA and OAPS/PSS, which is consistent with that indicated by UV. For the OAPS/PSS assembly, the average frequency changes associated with the adsorption of one OAPS layer was  $-304 \pm 25$  Hz and  $-113 \pm 15$  Hz with one PSS layer, and the masses of each

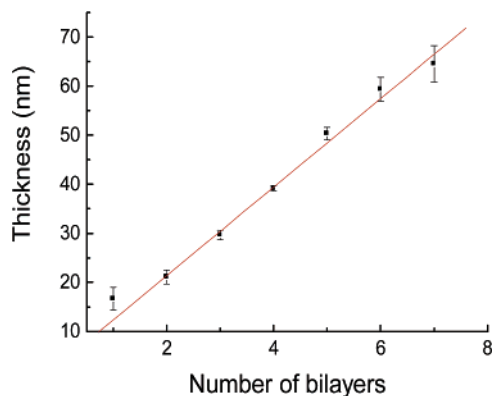


**Figure 9.** Thickness of the OAPS/PAA multilayer films as a function of the number of OAPS/PAA bilayers assembled obtained by ellipsometry.

adsorbed OAPS and PSS layer were  $830 \pm 68 \text{ ng/cm}^2$  and  $309 \pm 41 \text{ ng/cm}^2$ , respectively, by applying the Sauerbrey equation.<sup>30</sup> This corresponds to a 73:27 OAPS to PSS mass ratio, which agrees very well with the composition result based on XPS analysis. Furthermore, using the density data for bulk OPS ( $1.12 \text{ g/cm}^3$ ) and PSS ( $\sim 1.0 \text{ g/cm}^3$ ), it can be estimated that each OAPS layer contributed a thickness of  $7.4 \pm 0.6 \text{ nm}$ , and each PSS layer was  $3.1 \pm 0.4 \text{ nm}$  in the OAPS/PSS composite thin films. For the OAPS/PAA composite films, the average frequency changes associated with one OAPS layer was  $-299 \pm 21 \text{ Hz}$  and  $-56 \pm 5 \text{ Hz}$  with one PAA layer, which corresponds to an 84:16 OAPS to PAA mass ratio, which again is in good agreement with the composition data derived from the XPS atomic ratios discussed above. The average thicknesses of each OAPS layer and PAA layer (assuming a bulk density of  $1.1 \text{ g/cm}^3$ ) were then estimated to be  $7.3 \pm 0.5 \text{ nm}$  and  $1.4 \pm 0.1 \text{ nm}$ , respectively. In addition, the OAPS/PAA films were analyzed using ellipsometry, and the thickness of the film as a function of the number of the OAPS/PAA bilayers deposited is shown in Figure 9. It can be seen that the thickness growth is uniform, with the average thickness of each bilayer of  $9.0 \pm 1.0 \text{ nm}$ , which is coincident with the bilayer thickness estimated by QCM. The refractive index of the OAPS/PAA multilayer film was also determined by ellipsometry to be  $1.325 \pm 0.003$ , while for pure PAA the refractive index was  $1.510 \pm 0.001$ . The dielectric constant of a film can be estimated on the basis of the refractive index by applying the Maxwell equation,  $\epsilon \approx \eta^2$ , with a frequency dispersions correction,  $\Delta\epsilon \approx 0.3$ .<sup>32</sup> The dielectric constant thus derived for the OAPS/PAA composite film is 2.06 compared to 2.58 for the PAA film, showing a significant decrease due to the incorporation of the nanopores.

It has been shown in the literature that heat-induced amide formation between layer-by-layer assembled PAA and poly-(allylamine) layers can significantly increase its robustness.<sup>33</sup> This approach was applied to the assembled OAPS/PAA films. Figure 10 compares the 1900–1300  $\text{cm}^{-1}$  region of the reflection–absorption FTIR spectra of an OAPS/PAA film of nine bilayers on a PDDA/PAA-primed gold substrate

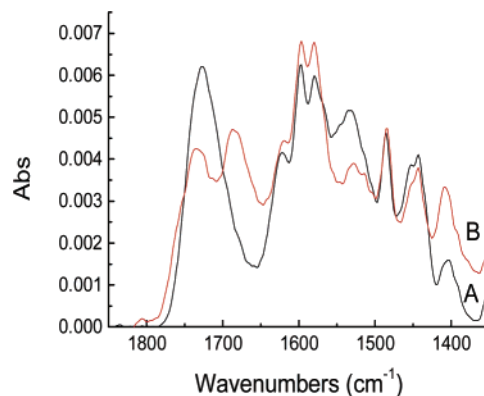


**Figure 10.** Reflection–adsorption FTIR spectra of an OAPS/PAA film with nine OAPS/PAA bilayers (A) before and (B) after heat treatment at  $205 \text{ }^\circ\text{C}$  for 2 h.

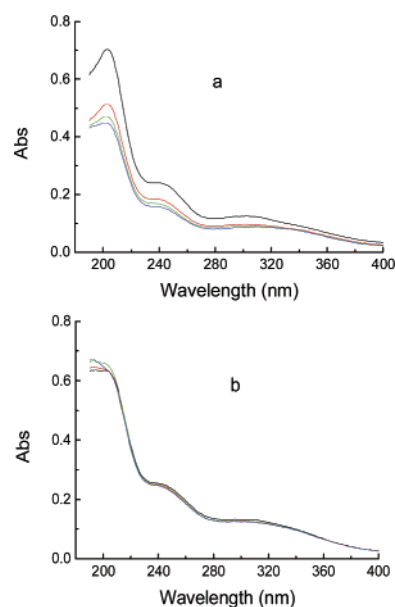


**Figure 11.** UV spectra of OAPS/PAA multilayer films, (a) without or (b) with heat treatment, after being immersed in HCl ( $\text{pH} = 0.6$ ) for 0, 12, 24, and 34 h (from top to bottom).

before and after being treated at  $205 \text{ }^\circ\text{C}$  for 2 h. It can be observed that after heating the intensity of the  $-\text{COO}^-$  stretching at  $1727 \text{ cm}^{-1}$  significantly decreases, and a new band at  $1685 \text{ cm}^{-1}$  appears, which may be assigned to the amide I vibration, suggesting the amide formation between the PAA and the OAPS. This conclusion was supported by XPS analysis, which revealed a new amide carbon component in the C 1s spectrum of the heated film (data not shown). No significant change in the surface topography of the film was observed by AFM after the heat treatment. To assess the effect of the heat treatment on the stability of the film, two OAPS/PAA composite films, one treated and the other a control, were immersed in an acid solution at  $\text{pH} \sim 0.6$ . The UV spectra (Figure 11) of these two films show that the acid caused extensive desorption of the assembled OAPS and PAA for the film without heat treatment, while essentially no desorption was found for the treated film in the acid for up to 34 h. This clearly demonstrates that there was extensive cross-linking between the OAPS and the PAA, presumably a result of the amide formation as suggested by the FTIR data, which significantly increased the stability of the film.

(32) Boese, D.; Lee, H.; Yoon, D. Y.; Swalen, J. D.; Rabolt, J. F. *J. Polym. Sci., Part B: Polym. Phys.* **1992**, *30*, 1321.

(33) Harris, J. J.; DeRose, P. M.; Bruening, M. L. *J. Am. Chem. Soc.* **1999**, *121*, 1978.

### Conclusions

In this paper we demonstrated that ultrathin composite films with low dielectric constants can be fabricated by incorporation of nanopores via layer-by-layer electrostatic self-assembly of OAPS with polyelectrolytes such as PAA. The OAPS synthesized was found to be soluble in water only at pH 3 or lower, which is not favorable for its electrostatic self-assembly with polyanions, especially when the polyanion is a weak polyelectrolyte such as PAA. Nevertheless suitable pH conditions were determined for the assembly of OAPS with PAA and PSS, and steady and uniform growth of OAPS/PAA and OAPS/PSS multilayers was observed. Under the assembly conditions explored, the major component of the composite films was the OAPS, which contributed more mass and thickness to the film and formed aggregates when deposited, resulting in a rough surface topography, while the PAA or PSS mainly filled in the gaps and valleys holding the OAPS clusters together like a glue without changing the surface topography much. The

incorporation of the porous OAPS into the thin films significantly lowered their dielectric constants. The OAPS/PAA composite films exhibited a dielectric constant of 2.06 compared to 2.58 for a pure PAA thin film. Furthermore, the stability of the OAPS/PAA multilayer composite films can be significantly improved by cross-linking between the OAPS and PAA layers via heat-induced amide formation. This process provides an easy approach to fabrication of ultrathin films with low dielectric constants.

**Acknowledgment.** We acknowledge the financial support from the National Natural Science Foundation of China (NSFC), the Ministry of Science and Technology, and the Jilin Distinguished Young Scholars Program.

**Supporting Information Available:** Elemental analysis results for ONPS (PDF). This material is available free of charge via the Internet at <http://pubs.acs.org>.

CM0607583